The Astrophysical Journal Letters, 793:L32 (5pp), 2014 October 1 doi:10.1088/2041-8205/793/2/L32

FIRST IMAGES FROM THE *FOCUSING OPTICS X-RAY SOLAR IMAGER*

Säm Krucker[1,2], Steven Christe[3], Lindsay Glesener[1], Shin-nosuke Ishikawa[4], Brian Ramsey[5], Tadayuki Takahashi[6,7], Shin Watanabe[6,7], Shinya Saito[6,7], Mikhail Gubarev[5], Kiranmayee Kilaru[5], Hiroyasu Tajima[8], Takaaki Tanaka[9], Paul Turin[1], Stephen McBride[1], David Glaser[1], Jose Fermin[1], Stephen White[10], and Robert Lin[1]

[1] Space Sciences Laboratory, University of California at Berkeley, Berkeley, CA, USA
[2] University of Applied Sciences and Arts Northwestern Switzerland, Windisch, Switzerland
[3] NASA Goddard Space Flight Center, Greenbelt, MD, USA
[4] National Astronomical Observatory, Mitaka, Japan
[5] NASA Marshall Space Flight Center, Huntsville, AL, USA
[6] Institute of Space and Astronautical Science (ISAS)/JAXA, Sagamihara, Japan
[7] Department of Physics, University of Tokyo, Tokyo, Japan
[8] Solar-Terrestial Environment Laboratory, Nagoya University, Nagoya, Japan
[9] Department of Physics, Kyoto University, Kyoto, Japan
[10] Air Force Research Laboratory, Albuquerque, NM, USA
Received 2014 June 10; accepted 2014 August 29; published 2014 September 15

ABSTRACT

The *Focusing Optics X-ray Solar Imager* (*FOXSI*) sounding rocket payload flew for the first time on 2012 November 2, producing the first focused images of the Sun above 5 keV. To enable hard X-ray (HXR) imaging spectroscopy via direct focusing, *FOXSI* makes use of grazing-incidence replicated optics combined with fine-pitch solid-state detectors. On its first flight, *FOXSI* observed several targets that included active regions, the quiet Sun, and a *GOES*-class B2.7 microflare. This Letter provides an introduction to the *FOXSI* instrument and presents its first solar image. These data demonstrate the superiority in sensitivity and dynamic range that is achievable with a direct HXR imager with respect to previous, indirect imaging methods, and illustrate the technological readiness for a spaceborne mission to observe HXRs from solar flares via direct focusing optics.

Key words: instrumentation: miscellaneous – Sun: corona – Sun: flares – Sun: X-rays, gamma rays

Online-only material: color figure

1. INTRODUCTION

Hard X-ray (HXR) observations are a powerful diagnostic tool for studying nonthermal electrons accelerated in solar flares (e.g., Kontar et al. 2011; Holman et al. 2011). HXRs are emitted from flare-accelerated electrons as they travel in the solar atmosphere and undergo bremsstrahlung collisions. Since bremsstrahlung intensity is proportional to the ambient plasma density, solar flare HXR emission is strongest at the footpoints of flare loops in the chromosphere, where high densities cause the energetic electron beams to thermalize (e.g., Fletcher et al. 2011).

Fainter HXR emission emanates from sources in the low densities of the corona, where acceleration of electrons and ions is thought to occur (e.g., Krucker et al. 2008a). While this particle acceleration is associated with the release of magnetic energy in the corona, the exact mechanisms that produce such efficient acceleration are not understood. The study of coronal HXRs provides information about energetic electron distributions during and after the acceleration process, but these sources are intrinsically faint and difficult to observe in the presence of bright footpoints (e.g., Masuda et al. 1994; Petrosian et al. 2002; Battaglia & Benz 2006). Investigation of flare electron acceleration therefore requires HXR observations with high sensitivity and dynamic range.

Currently, the most sensitive solar HXR images are provided by the *Reuven Ramaty High Energy Solar Spectroscopic Imager* (*RHESSI*) spacecraft (Lin et al. 2002). *RHESSI* uses rotation modulation collimation, a Fourier-based indirect imaging technique, to perform imaging spectroscopy (Hurford et al. 2002). With this technique, *RHESSI* achieves fine angular and spectral resolutions, down to 2.3 arcsec and 1 keV, respectively, over a wide energy range.

However, this technique is fundamentally limited in two important aspects. First, the instrument's effective area is directly proportional to detector area, and so the only ways to improve the sensitivity of a *RHESSI*-type instrument would be to build larger-area detectors, and/or to better shield the detectors. Both solutions are cost-intensive and cannot fit within the cost envelope of, for example, a Small Explorer class spacecraft.

Second, the imaging dynamic range of a *RHESSI*-like instrument is intrinsically limited since its modulation pattern is dominated by the brightest source in the field of view (FOV). In practice, *RHESSI* images typically show imaging reconstruction artifacts below about 20% of the maximum intensity, indicating a dynamic range of ∼5, with the exact value smaller or greater (sometimes up to ∼30) depending on counting statistics and source complexity. (Here, we have defined dynamic range as the ratio of the source intensity peak to the noise peak in the image.) This is generally insufficient to observe faint coronal HXRs expected from electrons in the presence of footpoint sources that are usually one to two orders of magnitude times brighter. As a consequence, *RHESSI* only occasionally observes HXR sources from the corona (see Sui & Holman 2003; Lin et al. 2003; Veronig & Brown 2004; Krucker et al. 2008b; Ishikawa et al. 2011a for notable examples from *RHESSI* observations) even though studies suggest that such sources should be present in essentially all flares (Krucker & Lin 2008). In short, present-day instruments lack the sensitivity to regularly measure faint HXR emission from flare-accelerated electrons in the corona (for example, from upward-directed electron beam emitting radio bursts; Saint-Hilaire et al. 2009) and the dynamic range to observe such faint emission in the presence of bright chromospheric footpoint sources.

Direct imaging, through focusing, can overcome both of these limitations. With direct focusing, collecting area is determined by the optics, not by detector size, meaning that detectors can be relatively small, dramatically reducing background flux, and can be easily shielded for further background reduction. The imaging dynamic range of a direct imager is also increased due to a point spread function (PSF) that characteristically falls monotonically and steeply with distance from the source centroid.

This direct focusing technique is well-established for soft X-ray astronomy, with the first demonstrations via rocket in the 1960s (Giacconi et al. 1965) and with tremendously successful space laboratories operating since the late 1990s (e.g., *Chandra* and *XMM-Newton*). More recently, direct focusing instruments dedicated for HXRs have flown on balloon platforms for astrophysical investigations, such as *HEFT*, *InFOCuS*, and *HERO* (Harrison et al. 2000; Ogasaka et al. 2005; Ramsey et al. 2002). Since 2012, the *Nuclear Spectroscopic Telescope Array* (*NuSTAR*), a spaceborne observatory, has observed astrophysical objects with a sensitivity over 100 times greater than that of previous HXR observers that used indirect methods (Harrison et al. 2013).

The *Focusing Optics X-ray Solar Imager* (*FOXSI*) experiment is a sounding rocket payload that demonstrates the suitability and technological readiness of direct focusing HXR optics for solar flare studies. *FOXSI* is the first project to apply HXR focusing optics to solar observation. Subsequent efforts have already begun, including a second *FOXSI* flight anticipated for 2014 December and the *HEROES* balloon (Christe et al. 2013), which flew in 2013 September. This Letter provides a brief introduction to the instrument, a description of the first flight, and the first focused HXR image of a solar microflare.

2. THE *FOXSI* PAYLOAD

FOXSI is funded under NASA's Low Cost Access to Space program. Hardware development for *FOXSI* took place at the Space Sciences Laboratory at UC Berkeley, the NASA/Marshall Space Flight Center (MSFC), and the Institute of Space and Astronautical Science (ISAS)/JAXA in Japan. Major components include replicated nickel optics and double-sided silicon strip detectors, described in Sections 2.1 and 2.2, respectively.

The scientific goal of *FOXSI*'s first flight was to perform a search for HXRs from non-thermal electrons in small nanoflares theorized to occur in the quiet regions of the Sun, i.e., outside flaring active regions (e.g., Klimchuk 2006). The best previous upper limits come from *RHESSI* measurements (Hannah et al. 2007, 2010), but to date this emission remains undetected. As a sounding rocket payload, *FOXSI* can achieve sufficient altitude (>150 km) and a long enough focal length (2 m) to observe HXRs from 4 to 15 keV, appropriate for studying nanoflare-accelerated electrons.

FOXSI achieves angular and energy resolutions of 8.8 ± 0.3 arcsec (on-axis) and 509 ± 74 eV, respectively, as measured in laboratory calibrations. With its direct HXR imaging, *FOXSI*'s nominal effective area is $\sim$100 cm^2 at 10 keV, an improvement of a factor of $\sim$3 as compared with *RHESSI*. Since *FOXSI*'s optics focus photons onto a finely segmented detector, the background is drastically reduced (by roughly four orders of magnitude for a flare measurement), providing an additional increase in sensitivity. *FOXSI* laboratory calibrations indicate an imaging dynamic range of $\sim$20 ($\sim$200) for sources separated by 15 (30) arcsec with no imaging deconvolution, as compared with *RHESSI*'s dynamic range of up to $\sim$30 (but typically around 5) for an image produced using the CLEAN algorithm, independent of source separation. Table 1 lists some key parameters for the instrument.

Table 1
Key *FOXSI* Parameters, from Laboratory Calibrations

Parameter	Measured Value
Focal length	2 m
Optics type	Wolter I
Number of optics modules	7
Number of mirror shells	7 per module, 49 total
Detector type	Double-sided Si strip
Strip pitch	75 μm
Detector dimensions	9.6×9.6 mm^2 (128×128 strips)
Angular resolution	
Detector strip pitch	7.7 arcsec (75 μm)
Optics PSF, FWHM	4.3 ± 0.6 arcsec (on-axis)[a]
	5.1 ± 0.4 arcsec (7 arcmin off-axis, long axis)[a,b]
	3.7 ± 0.4 arcsec (7 arcmin off-axis, short axis)[a,b]
Combined optics + detectors[c]	8.8 ± 0.3 arcsec (on-axis)[a]
	9.2 ± 0.2 arcsec (7 arcmin off-axis, long axis)[a,b]
	8.5 ± 0.2 arcsec (7 arcmin off-axis, short axis)[a,b]
Half power diameter	27.1 ± 1.7 arcsec (on-axis)
Field of view	16.5×16.5 arcmin^2 (detector area)
	$\sim$20 arcmin diameter (optics FWHM)
Energy range	$\sim$4 to 15 keV
Energy resolution	509 ± 74 eV
Nominal effective area	$\sim$100 cm^2 at 10 keV
	$\sim$10 cm^2 at 15 keV

Notes.
[a] Measurement of a single module; see Section 2.1.
[b] See Section 2.1 for a definition of the long and short axes.
[c] Optics PSF FWHM added in quadrature with detector strip pitch.

2.1. Optics

The *FOXSI* optics are monolithic nickel-alloy shells with a Wolter I geometry (Wolter 1952; Aschenbach 1985) containing parabolic and hyperbolic segments. The optics were fabricated at MSFC using an electroformed nickel replication (ENR) process. In this process, thin (250 μm) nickel-alloy mirror shells are electroformed onto superpolished electroless-nickel-plated aluminum figured mandrels, from which they are later separated by immersion in a cold bath (Ramsey 2006). Since figuring and polishing are performed on the mandrels and the replicated shells require no further polishing, ENR is a relatively low-cost alternative to conventional figuring and polishing of individual mirrors. The MSFC fabrication technique was developed for the *High Energy Replicated Optics* (*HERO*) balloon program (Ramsey et al. 2002). *HERO* has completed several flights and is an important source of heritage for *FOXSI*.

For increased effective area, mirror shells of different diameters are nested together into modules. Each diameter requires a different mandrel, so the project budget dictates the number of shells per module. *FOXSI* contains seven optics modules, each with seven nested shells, that provide effective area up to $\sim$15 keV. The focal length is limited to 2 m by the length

Table 2
FOXSI Targets

Target	Pointing (X, Y, arcsec)	Start	End	Duration (s)	Notable Features
1	−480, −350	17:56:48	17:57:32	44	AR 11602
2	−850, 150	17:57:35	17:59:05	90	AR 11604
3	600, 400	17:59:07	18:00:37	90	AR 11603, near edge of FOV
4	700, −600	18:00:40	18:03:18	140[a]	AR 11599, 11598, microflare

Note. [a] Not including 18 s of pointing adjustment.

constraints of a sounding rocket payload, which limits the effective area at high energies.

The angular resolutions of all the modules were measured prior to the flight using a single-pixel CdZnTe detector stepped across the focal plane. After the flight, one module was remeasured using a newly available CCD camera, producing a more precise measurement. The FWHM of the PSF measured with this new method was 4.3 ± 0.6 arcsec for an on-axis source. An off-axis source is elongated in the azimuthal direction and squeezed in the radial direction; postflight measurements found PSF FWHMs of 5.1 ± 0.4 and 3.7 ± 0.4 arcsec for a source located 7 arcmin off-axis. The measured half power diameter (HPD) is 27 ± 1.7 arcsec (on-axis). More detail on the fabrication and calibration of the *FOXSI* optics can be found in Glesener (2012) and Krucker et al. (2013). A plot of *FOXSI*'s PSF in comparison with other instruments can be found in Krucker et al. (2013).

2.2. Detectors

The focal-plane sensors for the *FOXSI* payload are double-sided silicon detectors (DSSDs) provided by ISAS/JAXA (Ishikawa et al. 2011b). The detectors were designed at ISAS/JAXA, drawing on heritage from detector development for the Hard X-ray Imager (HXI) on the *Astro-H* spacecraft (Kokubun et al. 2012; Takahashi et al. 2012). These detectors were fabricated by Hamamatsu Photonics by implanting orthogonal n- and p-doped strips on either side of a monolithic silicon wafer. Due to the orthogonality of the strips, measurement of the charge carriers (electrons and holes) provides a two-dimensional position of a photon energy deposition. The detectors are 500 μm thick and have a strip pitch of 75 μm, corresponding to an angular resolution of 7.7 arcsec at the focal length of 2 m. The system effective angular resolution (combining in quadrature the FWHM of the optics PSF and the detector strip pitch) is then 8.8 ± 0.3 arcsec for an on-axis source. Each side of the DSSD has 128 strips, for a total active area of 9.6×9.6 mm^2 corresponding to an FOV of 16.5×16.5 arcmin; this encompasses most of the optics' FOV (FWHM) of $\sim$20 arcmin.

Each telescope module is paired with a dedicated DSSD. The DSSDs are read out by low-power, low-noise ASICs developed by ISAS/JAXA in collaboration with Stanford University and Gamma Medica-Ideas (Tajima et al. 2004). These ASICs include fast and slow shapers (for triggering and measurement, respectively) and Wilkinson-style analog-to-digital converters (ADCs). For each energy deposition above the threshold, the ADC value of the strip with the maximum value and its two neighboring strips are recorded. Inclusion of the nearest neighbors ensures that full charge is collected in charge-shared events. For simplicity in onboard data handling, the system transmits a maximum rate of 500 events per second per detector. This rate is sufficient to measure the expected quiet-Sun HXR flux levels and could easily be raised for a future flare-dedicated mission with higher fluxes.

Each detector was calibrated in the laboratory using radioactive sources. The energy range with 25% efficiency or greater is 3.9–24.4 keV, with the lower and upper energies limited by a threshold set above the electronics noise and the efficiency of silicon photoabsorption, respectively. The energy resolution, as measured from the FWHM of the 13.9 keV line emitted by an americium source, is 509 eV (averaged over all flight detectors) with a standard deviation of 74 eV. More detail on the laboratory calibration of the detectors can be found in Glesener (2012) and Krucker et al. (2013).

2.3. Mechanical Structure

The optics and detectors are mounted at either end of a metering structure 2 m in length, cantilevered from the optics end (with six attachment points). In order to maintain the detectors at their optimal temperature ($\lesssim -15^\circ$C) during the entire observation, preflight cooling was provided from a liquid nitrogen dewar on the launch rail, cooling the detectors to between -32 and -28°C. The temperature during the flight was then maintained via thermal blanketing and an appropriate thermal mass within the detector package. Temperature sensors on the detector boards indicated that none of the boards reached a temperature higher than -23°C.

The alignment between the detectors and optics was measured using an X-ray generator and was found to be 40 arcsec or less for five modules, and up to 2.2 arcmin for the other two. Details of the alignment procedure can be found in Krucker et al. (2013). The alignment between the *FOXSI* optics and the rocket pointing system (provided by the NASA sounding rocket operations team), was measured using an autocollimator and was found to be $\sim$2 arcmin, an acceptable value since *FOXSI*'s science goals for the first flight did not require precise pointing.

3. FLIGHT

The *FOXSI* payload was launched from the White Sands Missile Range in New Mexico on 2012 November 2 at 17:55 UT. The payload reached an apogee of 340 km. Observations above 150 km (an altitude below which atmospheric absorption significantly attenuates 5 keV X-rays) began at 17:56:48 UT and lasted for 6.5 minutes. The instrument was recovered, intact, after the successful flight. Post-flight inspection of the payload showed that thermal blanketing infringed on the optical path during the solar observations and therefore significantly reduced sensitivity at lower energies. Preliminary comparison with the *RHESSI* spectrum shows that the effective area was reduced by a factor of at least $\sim$6 at the count spectrum peak of $\sim$6 keV. This additional absorption severely reduces the instrument sensitivity and requires a recalibration of the instrument response for photon spectroscopy, but does not change the image quality.

FOXSI observed a total of four solar targets, the details of which are listed in Table 2. Coordinated observations with *Hinode* of active region (AR) 11602 are presented by Ishikawa et al.

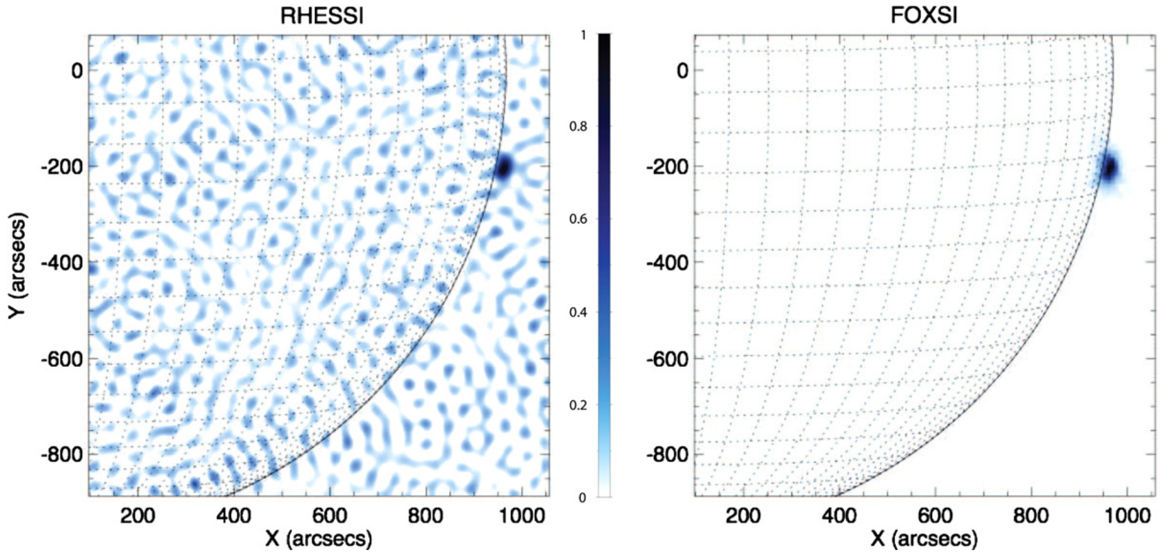

Figure 1. Comparison of *RHESSI* (left) and *FOXSI* (right) images of a B2.7 microflare during *FOXSI*'s first flight on 2012 November 2. The *RHESSI* image was produced using the CLEAN imaging algorithm with subcollimators 3–9; typical image reconstruction artifacts are visible across the entire image. Since *FOXSI* is a direct imager, the image on the right does not include this imaging noise and has a much improved imaging dynamic range. The *FOXSI* image, using data from a single optic/detector pair, shows the instrument's entire field of view, while the *RHESSI* image has been restricted to the same field of view as that of *FOXSI*. The same color table and scaling is used in both images.

(A color version of this figure is available in the online journal.)

(2014) and show that *FOXSI*'s high-sensitivity observations provide new constraints on the presence of a high-temperature component in active regions. In the first three targets, an average rate of 1–2 counts per second was distributed across the entire FOV. This flux could come from focused solar sources, singly reflected (stray) photons from a flaring region outside the FOV, or nonsolar background, providing an upper limit for the nonsolar background. For a flare study, a relevant background would be the detector area corresponding to the HPD of the optics. From the flight data, an upper limit on the nonsolar background within the HPD is 6×10^{-4} counts s^{-1} keV^{-1} within 4–15 keV, which would be negligible for all previously detected flares.

In the fourth and final target, *FOXSI* observed a microflare (SOL2012-11-02T17:59; *GOES* class B2.7 after background subtraction) associated with AR 11598 at the western limb. A simultaneous *RHESSI* observation shows an extended thermal source above the limb. *RHESSI* image reconstruction depends on the choice of subcollimators, which measure different spatial frequencies (Hurford et al. 2002). Here, the finest subcollimator (2.3 arcsec) shows no measurable modulation, indicating no detectable source structure at that spatial scale. The detector behind the second subcollimator was not functional at these low energies at the time of *FOXSI*'s flight, so the best *RHESSI* image is attained using subcollimators 3–9, corresponding to an angular resolution of 9.8 arcsec. Figure 1 shows a comparison of the image of the microflare made by *RHESSI* (produced using the CLEAN imaging algorithm) and an image produced using raw *FOXSI* counts from one detector. *FOXSI*'s pointing was corrected by the coalignment of the flare locations as measured by *FOXSI* and *RHESSI*, a difference of approximately 2 arcmin. The excess of imaging artifacts in the *RHESSI* reconstruction as compared with the *FOXSI* raw image is evident.

A cut across the *FOXSI* image shows that the flux drops to 10% of its maximum (a dynamic range of 10) within 26 arcsec and 1% (a dynamic range of 100) within 47 arcsec. This is an underestimate of the true dynamic range because of the finite size of the flare, i.e., the flux profile is a convolution of the PSF with the flare morphology. *RHESSI*'s dynamic range for this event (which is a small event with poor statistics) is ∼3. To get an in-flight measurement of the *FOXSI* PSF, an observation of a point source would be required. The observed microflare source is spatially extended and a simple direct measurement of the PSF is therefore not possible. A following paper will extend these preliminary results by deconvolving the PSF from the *FOXSI* microflare images and will present a more detailed comparison with the *RHESSI* images.

The microflare occurred at an off-axis location of 7.3 arcmin from the optical axis, so the optics response is slightly degraded. The optics PSF becomes elongated, with FWHMs of 5.1 ± 0.4 and 3.7 ± 0.4 arcsec in the azimuthal and radial directions for an off-axis source position of ∼7 arcmin. Combined with the detector strip pitch, this corresponds to an angular resolution of ∼9 arcsec. At this off-axis position, the throughput is 70% of its on-axis value.

Figure 2 shows a *FOXSI* count spectrum for the data shown in Figure 1, including all counts within 50% of the maximum on a raw image of 3–15 keV counts. The dashed line shows the background spectrum at a distant location from the flaring site, scaled to the same area, demonstrating the ability to easily perform imaging spectroscopy within a single image. The true background for a nonflaring Sun is likely even lower than this curve since the measured data include some flux from the wings of the optics' response to the flare. A fully calibrated photon spectrum is not presented here because its determination requires an extensive recalibration of the instrument response to account for the excess blanketing; a following paper will present that analysis. That recalibration does not affect the quality of the image shown in Figure 1, nor does it affect the ratio of intensities of the flaring and nonflaring Sun shown in Figure 2.

4. SUMMARY

FOXSI's first flight was a comprehensive success, obtaining both HXR images and spectra. This Letter reports an initial, unprocessed image. A following paper will provide a detailed

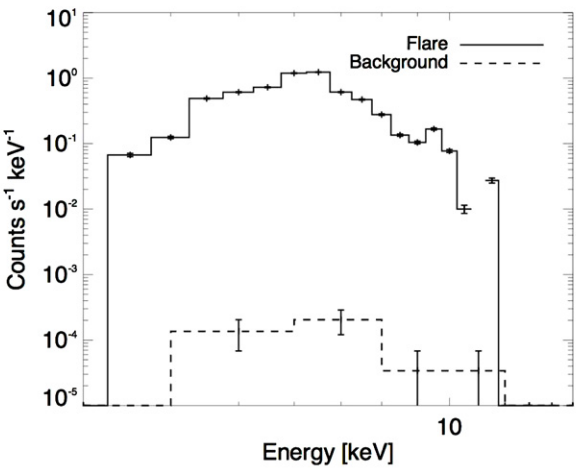

Figure 2. *FOXSI* microflare count spectrum, as measured within a 50% contour on the raw image for one detector. The dashed line shows the background spectrum measured in a nonflaring section of the same image (center [500, −700] arcsec with radius 200 arcsec), scaled to the same area as that used for the flare spectrum. The difference between the two curves (>three orders of magnitude) is an indication of the large dynamic range.

comparison of images and spectra with *RHESSI*, including results from the other detectors. These observations constitute the first focused images of the Sun above 5 keV and demonstrate the unique capabilities of high-energy grazing incidence optics for solar observations.

The *FOXSI* payload will fly again in late 2014. Since the payload was recovered, intact, much of the system will be reused. Optics and detector upgrades will increase effective area, mainly at higher energies. New thermal analysis shows that the inner thermal blankets are unnecessary, and so they will be removed as to avoid impinging on the optical path. The combined effect is expected to increase the sensitivity relative to the first *FOXSI* payload by an order of magnitude at low energies (∼5 keV).

A future space-based observatory featuring similar technology would perform systematic observations of HXR flares with far greater sensitivity and imaging dynamic range than those of current instruments. Such an instrument would be able to systematically investigate the role of nanoflares in coronal heating; could quantitatively investigate coronal acceleration sites, pinpointing the acceleration region and constraining acceleration models; and could image outward-directed electron populations associated with coherent radio bursts and coronal mass ejections. The success of *FOXSI*'s first flight demonstrates that the focusing technology necessary for such a spaceborne solar observatory is mature and ready for implementation.

FOXSI was funded by NASA LCAS grant NNX08AH42G and received support from NASA GSRP fellowship NNX09AM40H. *RHESSI* work is supported by NASA contract NAS 5-98033. The team is grateful to JAXA/ISAS for the donation of detectors and ASICs. We thank the numerous members of the NSROC teams at WSMR and Wallops for the excellent operation of their systems. We also thank the numerous members of the *RHESSI* and SSL communities who contributed advice and help to the project, particularly Hugh Hudson and Gordon Hurford for providing helpful advice on this Letter.

This work is dedicated to the memory of Bob Lin, who initiated the *FOXSI* collaboration.

REFERENCES

Aschenbach, B. 1985, RPPh, 48, 579
Battaglia, M., & Benz, A. O. 2006, A&A, 456, 751
Christe, S. D., Shih, A., Rodriguez, M., et al. 2013, Proc. SPIE, 8862, 886206
Fletcher, L., Dennis, B. R., Hudson, H. S., et al. 2011, SSRv, 159, 19
Giacconi, R., Reidy, W. P., Zehnpfennig, T., Lindsay, J. C., & Muney, W. S. 1965, ApJ, 142, 1274
Glesener, L. E. 2012, PhD thesis, Univ. California, Berkeley
Hannah, I. G., Hudson, H. S., Hurford, G. J., & Lin, R. P. 2010, ApJ, 724, 487
Hannah, I. G., Hurford, G. J., Hudson, H. S., Lin, R. P., & van Bibber, K. 2007, ApJL, 659, L77
Harrison, F. A., Boggs, S. E., Bolotnikov, A. E., et al. 2000, Proc. SPIE, 4012, 693
Harrison, F. A., Craig, W. W., Christensen, F. E., et al. 2013, ApJ, 770, 103
Holman, G. D., Aschwanden, M. J., Aurass, H., et al. 2011, SSRv, 159, 107
Hurford, G. J., Schmahl, E. J., Schwartz, R. A., et al. 2002, SoPh, 210, 61
Ishikawa, S., Krucker, S., Takahashi, T., & Lin, R. P. 2011a, ApJ, 737, 48
Ishikawa, S., Saito, S., Tajima, H., et al. 2011b, ITNS, 58, 2039
Ishikawa, S., Glesener, L., Christe, S., et al. 2014, PASJ, in press
Klimchuk, J. A. 2006, SoPh, 234, 41
Kokubun, M., Nakazawa, K., Enoto, T., et al. 2012, Proc. SPIE, 8443, 844325
Kontar, E. P., Brown, J. C., Emslie, A. G., et al. 2011, SSRv, 159, 301
Krucker, S., Battaglia, M., Cargill, P. J., et al. 2008a, A&ARv, 16, 155
Krucker, S., Christe, S., Glesener, L., et al. 2013, Proc. SPIE, 8862, 88620R
Krucker, S., Hurford, G. J., MacKinnon, A. L., Shih, A. Y., & Lin, R. P. 2008b, ApJL, 678, L63
Krucker, S., & Lin, R. P. 2008, ApJ, 673, 1181
Lin, R. P., Dennis, B. R., Hurford, G. J., et al. 2002, SoPh, 210, 3
Lin, R. P., Krucker, S., Hurford, G. J., et al. 2003, ApJL, 595, L69
Masuda, S., Kosugi, T., Hara, H., Tsuneta, S., & Ogawara, Y. 1994, Natur, 371, 495
Ogasaka, Y., Tueller, J., Yamashita, K., et al. 2005, Proc. SPIE, 5900, 217
Petrosian, V., Donaghy, T. Q., & McTiernan, J. M. 2002, ApJ, 569, 459
Ramsey, B. D. 2006, AdSpR, 38, 2985
Ramsey, B. D., Alexander, C. D., Apple, J. A., et al. 2002, ApJ, 568, 432
Saint-Hilaire, P., Krucker, S., Christe, S., & Lin, R. P. 2009, ApJ, 696, 941
Sui, L., & Holman, G. D. 2003, ApJL, 596, L251
Tajima, H., Nakamoto, T., Tanaka, T., et al. 2004, ITNS, 51, 842
Takahashi, T., Mitsuda, K., Kelley, R., et al. 2012, Proc. SPIE, 8443, 84431Z
Veronig, A. M., & Brown, J. C. 2004, ApJL, 603, L117
Wolter, H. 1952, AnP, 445, 94